Probing the Sterile Neutrino Dipole Portal via Low-Energy Electron Recoils at Direct Detection Experiments

M F Mustamin[1] and M Demirci [2] *

[1]*Graduate School of Natural and Applied Science, Karadeniz Technical University, Trabzon 61080, Türkiye*
[2]*Department of Physics, Karadeniz Technical University, Trabzon, TR61080, Türkiye*

Abstract

We probe the sterile neutrino dipole portal via low-energy electronic recoil data from rent direct detection experiments. We provide limits on the active-sterile neutrino transition magnetic moments from the PandaX-4T and XENONnT dataset. Performing detailed statistical analyses, we derive the one degree of freedom limits of the dipole portal. Direct detections offer a unique framework for studying all possible neutrino flavors. This is achieved by using different neutrino flavors from the solar neutrino probability.

Keywords: sterile neutrino, dipole portal, direct detection experiment
DOI: 10.31526/BSM-2025.2

1. INTRODUCTION

After neutrino oscillations were discovered at Super-Kamiokande [1] and Sudbury National Observatory [2], evidence that neutrinos possess nonzero masses was revealed. This fact indicates a clear contradiction to the standard model (SM) prediction, where neutrinos are considered to be massless. These results, therefore, require a theory beyond the SM (BSM). In many extensions, neutrino masses can be described by the existence of an additional state, the sterile neutrino [3, 4].

On the other hand, direct detection (DD) experiments to search for dark matter (DM) are currently undergoing rapid advancements. Such facilities are typically located deep underground to significantly reduce cosmic ray backgrounds and other cosmogenic radiations. DM-DD experiments' main goal is to search for DM candidates. It potentially comes from recoil energy signals as DM particles interact with the materials of the detector target.

In DM-DD experiments, neutrinos constitute an irreducible background. It therefore offers a unique framework to explore the properties of neutrinos. Particularly, these kinds of experiments enable the study of solar neutrino interactions, allowing precision measurements of the weak mixing angle in the SM at the lowest accessible energies, and provide sensitivity to potential contributions from BSM regarding new neutrino interactions, where we consider the sterile neutrino dipole portal in this work.

The up-scattering process [5] is one possible way to produce sterile neutrinos. In this process, active neutrinos scatter off electrons in target material via transition magnetic moments [6]. This process is also known as the Primakoff scattering, where it is originally proposed to investigate neutral meson photoproductions [7]. We investigate the process through signals of electronic recoils at DM-DD experiments from the elastic neutrino-electron scattering (EνES) process. It gives a unique way to derive active-sterile neutrino transition magnetic moment limits. In this regard, we consider the datasets of PandaX-4T [8] and XENONnT [9] to derive limits on the transition magnetic moment of the sterile neutrino dipole portal. This proceeding is based on our recent work in Ref. [10].

We arrange the remainder of this paper as follows. The theoretical background is explained in Sec. 2. The χ^2–analysis used in this work is given in Sec. 3. The results of our work are in Sec. 4. Finally, the summary of our work is in Sec. 5.

2. THEORETICAL BACKGROUND

The sterile neutrino is a singlet under the electroweak theory. The particle is insensitive to the SM gauge bosons but potentially mixes with active neutrinos. The incorporation of the sterile neutrino can explain the smallness of active neutrino masses. For sterile neutrinos with a mass range in the keV–GeV scale, they can mix with active neutrinos and acquire transition dipole moments large enough to be observable [11]. This prospect offers unique frameworks for observations, enabling neutrinos to participate in EM interactions with the means of photon-mediated scattering or radiative decays. These kinds of processes are highly distinguishable in experiments, often indicated by clean single-photon signals or deviations of recoil spectra at low energies. This work focuses on the latter, particularly in the low-energy electronic recoils at DM-DD experiments.

The sterile neutrino dipole portal, denoted by $\mu_{\nu_{\ell 4}}$, is an effective field theory where a dimension-five operator couples an active neutrino to a heavy neutral lepton through the EM field tensor $F_{\mu\nu}$. Its theoretical appeal lies in its minimality, as the entire phenomenology is governed by the dipole portal. It is robust, since dipole operators naturally appear in the effective Lagrangian, once heavy fields are integrated out. Explicitly, for SM extended with sterile fermions, the sterile dipole portal comes from the higher-dimensional operator $\frac{c}{\Lambda^2}(\overline{L}\sigma^{\mu\nu}\nu_4)\tilde{H}B_{\mu\nu}$ [11, 12]. Here, $\sigma^{\mu\nu} = i[\gamma^\mu, \gamma^\nu]/2$, $L = (\nu_{\ell L}, \ell_L)^T$ is the SM lepton, $H = (\phi^+, \phi^0)^T$ the Higgs doublet, $B_{\mu\nu}$ the hypercharge field strength, and ν_4 the sterile neutrino, while c is a constant and Λ the heavy scale.

The effective operator for the sterile neutrino dipole portal at low-energy is expressed by

$$\mathcal{L}_{\rm int} \supset \frac{\mu_{\nu_{\ell 4}}}{2}\bar{\nu}_{\ell L}\sigma^{\mu\nu}P_R\nu_4 F_{\mu\nu} + \text{h.c.}, \tag{1}$$

*Corresponding author: mehmetdemirci@ktu.edu.tr

where P_R is the right-handed projection operator. It is obtained after electroweak (EW) symmetry breaking, where we can see the relation $\mu_{\nu_{\ell 4}} \approx cv/\Lambda^2$. This kind of interaction can be investigated within the framework of electromagnetically upscattered neutrino beams on electrons. Note that this effective form is suitable only at low energies, less than the EW scale. The electronic recoil signal, from the EνES process, involves neutrinos with relatively low energies, so that this is applicable. From this term, we obtain the differential cross-section as

$$\left[\frac{d\sigma(E_\nu, T_e)}{dT_e}\right] = \frac{\pi\alpha_{\rm EM}^2}{m_e^2}\left|\frac{\mu_{\nu_{\ell 4}}}{\mu_B}\right|^2\left[\frac{1}{T_e} - \frac{1}{E_\nu} - \frac{m_4^2}{2T_eE_\nu m_e}\left(1 - \frac{T_e}{2E_\nu} + \frac{m_e}{2E_\nu}\right) - \frac{m_4^4}{8m_eT_e^2E_\nu^2}\left(1 - \frac{T_e}{m_e}\right)\right]. \quad (2)$$

Here, $\pi\alpha_{\rm EM}/m_e^2$ is the magnetic moments as the Bohr magneton, μ_B. In the limit $m_4 = 0$, the expression reduces to the standard scenario involving only active neutrino scattering. In addition, there exists a kinematic constraint on the sterile neutrino mass. The contribution from an active–sterile neutrino transition magnetic moment adds coherently to the SM elastic neutrino–electron scattering, potentially enhancing the predicted event rate at low-energy electron recoils.

Neutrinos experience flavor oscillations while propagating from the Sun to the Earth. This implies solar neutrinos arrive at the detector as a mixture of all possible flavors. Consequently, the differential cross section needs to be multiplied by the solar neutrino survival probabilities

$$\left[\frac{d\sigma}{dT_e}\right]_X^{\nu e} = P_{ee}\left[\frac{d\sigma_{\nu_e}}{dT_e}\right]_X + \sum_{f=\mu,\tau} P_{ef}\left[\frac{d\sigma_{\nu_f}}{dT_e}\right]_X. \quad (3)$$

For ν_e, the survival probability is denoted by P_{ee}, while for an initial ν_e converting into a ν_f flavor ($f = \mu, \tau$), the survival probability is P_{ef}. These transition probabilities are given by $P_{e\mu} = (1 - P_{ee})\cos^2\vartheta_{23}$ and $P_{e\tau} = (1 - P_{ee})\sin^2\vartheta_{23}$, respectively. The electron neutrino survival probability, accounting for both vacuum and matter effects, is expressed as [13]

$$P_{ee} = \cos^2(\vartheta_{13})\cos^2(\vartheta_{13}^m)\left(\frac{1}{2} + \frac{1}{2}\cos(2\vartheta_{12}^m)\cos(2\vartheta_{12})\right) + \sin^2(\vartheta_{13})\sin^2(\vartheta_{13}^m), \quad (4)$$

where the neutrino mixing angles are denoted by ϑ_{12}, ϑ_{13}, and ϑ_{23}, while the superscript m indicates quantities evaluated in the solar matter environment. In our calculations, we include the day–night asymmetry arising from the regeneration of ν_e via coherent forward scattering with the Earth's matter during nighttime propagation. We adopt the normal mass ordering for the neutrino oscillation parameters, which are taken from the global three-flavor fit provided by NuFit 5.3 [14], excluding the Super-Kamiokande atmospheric neutrino dataset.

3. χ^2–FUNCTION

We calculate the predicted number of events in the k^{th} electron recoil energy bin is calculated as

$$R_X^k = \varepsilon N_t \int_{T_e^k}^{T_e^{k+1}} dT_e\, \mathcal{A}(T_e) \int_0^{T_e'^{\max}} dT_e'\, \mathcal{R}(T_e, T_e') \times \sum_{i=pp,^7{\rm Be}} \left[\frac{dR}{dT_e'}\right]_X^i, \quad (5)$$

where N_t is the number of target electrons per unit detector mass. The variables T_e and T_e' denote the reconstructed and true electron recoil energies, respectively, while ε denotes the exposure factor. The detector efficiency is given by the functions $\mathcal{A}(T_e)$, and the energy resolution function is given by $\mathcal{R}(T_e, T_e')$, considered to be equivalent to a Gaussian smearing. The variable dR/dT_e' is the differential event rate per unit target mass. We need to account for the number of available electrons per recoil energy bin to calculate this. The required minimum neutrino energy to produce a recoil energy with an outgoing sterile neutrino is

$$E_\nu^{\min} = \frac{T_e}{2}\left(1 + \sqrt{1 + \frac{2m_e}{T_e}}\right)\left(1 + \frac{m_4^2}{2m_eT_e}\right), \quad (6)$$

while the maximum energy $E_{\nu,i}^{\max}$ is taken from the neutrino flux endpoint.

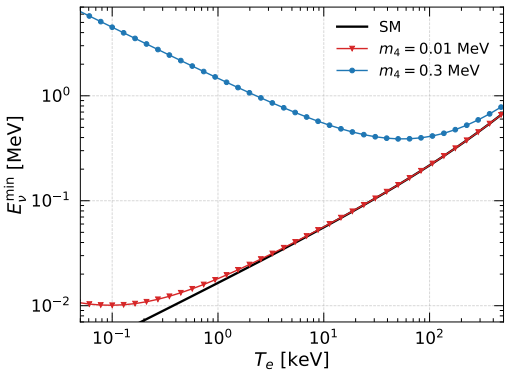

FIGURE 1: The minimum neutrino energy dependency with the electron recoil energy for $m_4 = 0.01$ (triangle-red line) MeV and $m_4 = 0.3$ MeV (circle-blue line). We also show the active-neutrino case (solid-black line).

To derive constraints on the new physics parameter(s) of interest, denoted by $\mathcal{S}$, we employ a Poisson-based χ^2 test statistic, which is defined as

$$\chi^2(\mathcal{S}) = \min_{(\alpha_i,\beta_j)} 2\sum_{k=1}^{30}\left[R_{\rm exp}^k(\mathcal{S};\alpha,\beta) - R_{obs}^k + R_{obs}^k \ln\left(\frac{R_{obs}^k}{R_{\rm exp}^k(\mathcal{S};\alpha,\beta)}\right)\right] + \sum_i\left(\frac{\alpha_i}{\sigma_{\alpha_i}}\right)^2 + \sum_j\left(\frac{\beta_j}{\sigma_{\beta_j}}\right)^2, \quad (7)$$

where $R_{\rm obs}^k$ and $R_{\rm exp}^k$ represent the observed and expected event rates in the k^{th} energy bin, respectively. The expected rate

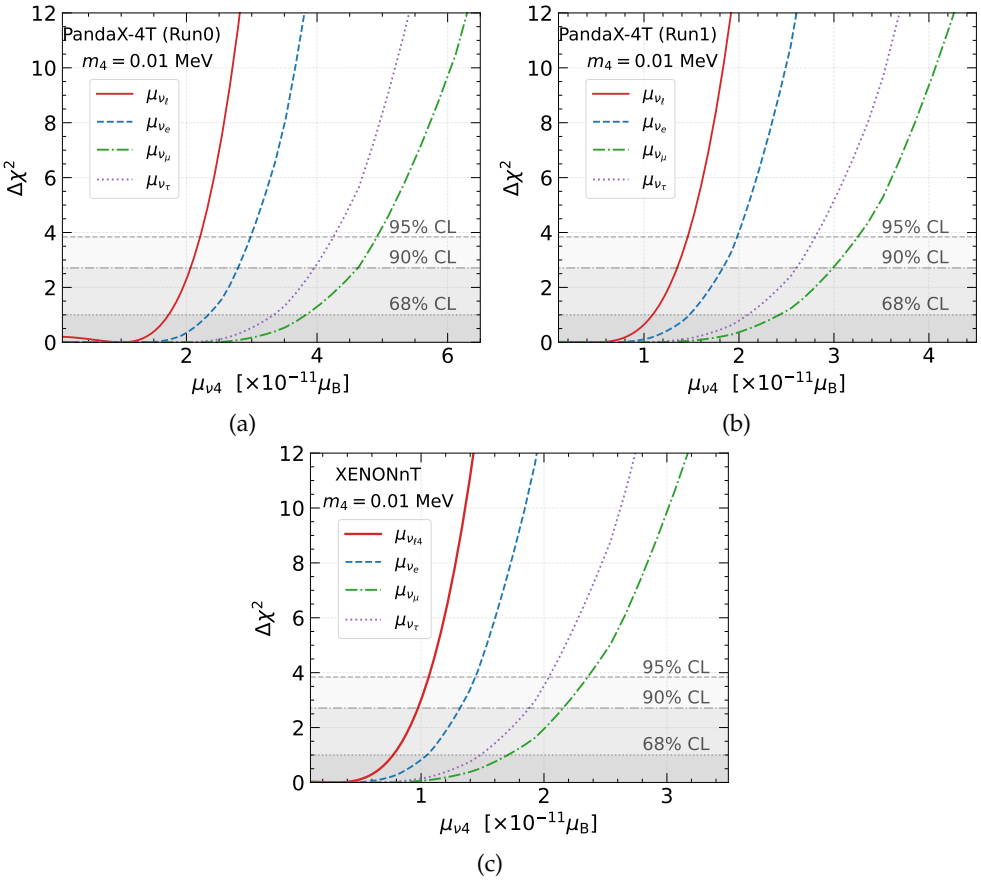

FIGURE 2: The likelihood profile of the active-sterile neutrino transition magnetic moment, derived from datasets of PandaX-4T Run0 (a), PandaX-4T Run1 (b), and XENONnT (c) for $m_4 = 0.01$ MeV.

consists of SM prediction $R^k_{\rm SM}$, the contribution from the transition magnetic moment $R^k_{\rm TMM}$, and other background components $R_{\rm Bkg}$. The variable α_i represents nuisance parameters corresponding to the solar neutrino flux uncertainties and β_j the individual background components. We have calculated the total event rate prediction, where both the SM and active-sterile neutrino transition magnetic moment are included, using solar neutrino fluxes from Bahcall's spectrum [15], normalized according to the B16-GS98 Standard Solar Model [16].

4. RESULTS

By setting two different sterile neutrino masses, we present the 1 dof limits with 90% CL of the active-sterile neutrino magnetic moment. We set $m_4 = 0.001$ MeV and $m_4 = 0.3$ MeV. We plot the dependence of minimum neutrino energy on electron recoil energy to see the behavior of the two selected sterile masses in Fig. 1. We can observe that the required minimum neutrino energy to produce an electronic recoil is linearly dependent on the increasing recoil energy. For $m_4 = 0.01$ MeV (circle-blue line), the spectrum approaches the active-only, massless neutrino case (solid-black line). The $m_4 = 0.3$ MeV (triangle-red line) case indicates larger neutrino energies required.

We now discuss our obtained limits with 90%CL with 1 dof for the two sterile neutrino masses. For $m_4 = 0.01$ MeV, we show our result in Fig. 2. Our obtained limits for PandaX-4T Run0 are $\mu_{\nu_{\ell 4}} \lesssim 2.06 \times 10^{-11}\mu_B$, $\mu_{\nu_{e4}} \lesssim 2.79 \times 10^{-11}\mu_B$, $\mu_{\nu_{\mu 4}} \lesssim 4.62 \times 10^{-11}\mu_B$, and $\mu_{\nu_{\tau 4}} \lesssim 3.96 \times 10^{-11}\mu_B$, which can be seen in Fig. 2.(a). Limits for PandaX-4T Run1 are in Fig. 2.(b), where we find $\mu_{\nu_{\ell 4}} \lesssim 1.35 \times 10^{-11}\mu_B$, $\mu_{\nu_{e4}} \lesssim 1.83 \times 10^{-11}\mu_B$, $\mu_{\nu_{\mu 4}} \lesssim 2.99 \times 10^{-11}\mu_B$, and $\mu_{\nu_{\tau 4}} \lesssim 2.60 \times 10^{-11}\mu_B$. For XENONnT, we can see in Fig. 2.(c) the limits are $\mu_{\nu_{\ell 4}} \lesssim 0.97 \times 10^{-11}\mu_B$, $\mu_{\nu_{e4}} \lesssim 1.32 \times 10^{-11}\mu_B$, $\mu_{\nu_{\mu 4}} \lesssim 2.15 \times 10^{-11}\mu_B$, and $\mu_{\nu_{\tau 4}} \lesssim 1.88 \times 10^{-11}\mu_B$. In Fig. 3, we show our results for $m_4 = 0.3$ MeV. Our results for PandaX-4T Run0 can be seen in Fig. 3.(a), where we find $\mu_{\nu_{\ell 4}} \lesssim 1.94 \times 10^{-11}\mu_B$, $\mu_{\nu_{e4}} \lesssim 2.68 \times 10^{-11}\mu_B$, $\mu_{\nu_{\mu 4}} \lesssim 4.48 \times 10^{-11}\mu_B$, and $\mu_{\nu_{\tau 4}} \lesssim 3.85 \times 10^{-11}\mu_B$. Results for PandaX-4T Run1 are in Fig. 3.(b), with $\mu_{\nu_{\ell 4}} \lesssim 1.54 \times 10^{-11}\mu_B$, $\mu_{\nu_{e4}} \lesssim 2.66 \times 10^{-11}\mu_B$, $\mu_{\nu_{\mu 4}} \lesssim 4.45 \times 10^{-11}\mu_B$, and $\mu_{\nu_{\tau 4}} \lesssim 3.85 \times 10^{-11}\mu_B$. Meanwhile for XENONnT, the results are in Fig. 3.(c) with $\mu_{\nu_{\ell 4}} \lesssim 8.45 \times 10^{-11}\mu_B$, $\mu_{\nu_{e4}} \lesssim 1.19 \times 10^{-11}\mu_B$, $\mu_{\nu_{\mu 4}} \lesssim 1.99 \times 10^{-11}\mu_B$, and $\mu_{\nu_{\tau 4}} \lesssim 1.72 \times 10^{-11}\mu_B$.

From these findings, we can clearly observe that the PandaX-4T Run1 data provide an improvement in sensitivity over PandaX-4T Run0. On the other hand, XENONnT data maintains competitive limits within the sterile mass values considered in this work. Our results strengthen the complementarity of the results from DM-DD experiments with other experimental facilities in studying the sterile neutrino dipole portal. Recent advancements of current-generation DM-DD experiments, together with expected facilities in the near-future, promise continued progress in the active-sterile neutrino transition magnetic moment.

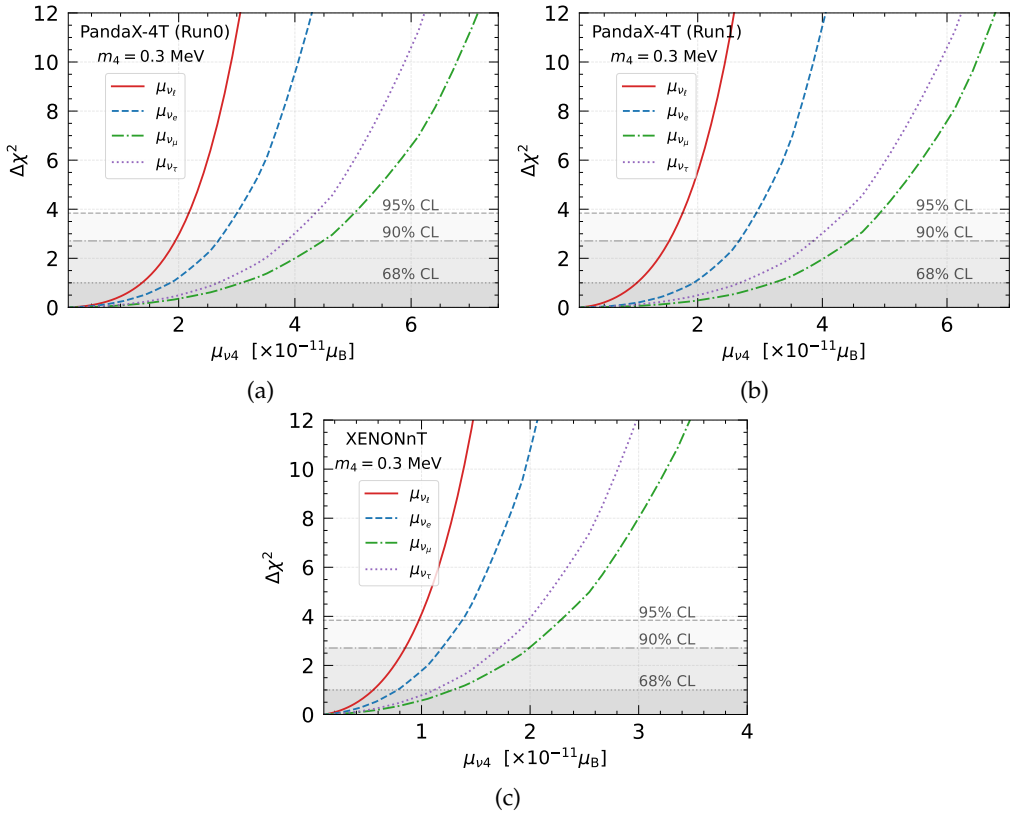

FIGURE 3: The likelihood profile of the active-sterile neutrino transition magnetic moment, derived from datasets of PandaX-4T Run0 (a), PandaX-4T Run1 (b), and XENONnT (c) for $m_4 = 0.3$ MeV.

5. SUMMARY

In this work, we have probed the sterile neutrino dipole portal and derived parameter limits from DM-DD experiments. Particularly, we used PandaX-4T (Run0 and Run1) and XENONnT electronic recoil data. The contribution of the active-sterile neutrino transition magnetic moment has been embedded in the solar-neutrino induced EνES process. It is one of the irreducible backgrounds in DM-DD experiments and offers a unique framework to study BSM physics in general. We have obtained limits at 1 dof of the sterile neutrino dipole portal by performing a robust statistical method. In general, the XENONnT dataset provide a more sensitive limits than the PandaX-4T. Our results indicate the capability of currently developed DM-DD experiments in exploring the sterile neutrino dipole portal in particular and BSM physics in general in a complementary and competitive manner.

ACKNOWLEDGEMENTS

This work was supported by the Scientific and Technological Research Council of Türkiye (TUBITAK) under the project no: 124F416.

References

[1] Y. Fukuda *et al.* (Super-Kamiokande Collaboration), Phys. Rev. Lett. **81**, 1562-1567 (1998).
[2] Q. R. Ahmad *et al.* (SNO Collaboration), Phys. Rev. Lett. **87**, 071301 (2001).
[3] B. Pontecorvo, Zh. Eksp. Teor. Fiz. **53**, 1717-1725 (1967).
[4] B. Dasgupta and J. Kopp, Phys. Rept. **928**, 1-63 (2021).
[5] G. Domokos and S. Kovesi-Domokos, Phys. Rev. D **55**, 2526-2529 (1997).
[6] D. McKeen, and M. Pospelov, Phys. Rev. D **82**, 113018 (2010).
[7] H. Primakoff, Phys. Rev. **81**, 899 (1951).
[8] X. Zeng *et al.* (PandaX Collaboration), Phys. Rev. Lett. **134**, 041001 (2025).
[9] E. Aprile *et al.* (XENON Collaboration), Phys. Rev. Lett. **129**, 161805 (2022).
[10] M. F. Mustamin and M. Demirci, [arXiv:2511.00701 [hep-ph]].
[11] S. K. Kang and C. J. Ouseph, Int. J. Mod. Phys. A, 2530022 (2025).
[12] R. Beltrán, P. D. Bolton, F. F. Deppisch, C. Hati and M. Hirsch, JHEP, **07** 153 (2024).
[13] M. Maltoni and A. Y. Smirnov, Eur. Phys. J. A **52**, 87 (2016).
[14] I. Esteban, M. C. Gonzalez-Garcia, M. Maltoni, T. Schwetz, and A. Zhou, J. High Energ. Phys **2020**, 178 (2020).
[15] J. N. Bahcall, Neutrino Astrophysics, Cambridge University Press (1989), ISBN: 9780521379755.
[16] N. Vinyoles, A. M. Serenelli, F. L. Villante, S. Basu, J. Bergström, M. C. Gonzalez-Garcia, M. Maltoni, C. Peña-Garay and N. Song, Astrophys. J. **835**, 202 (2017).